# Electronic and optical excitations in $Ag_n$ clusters ($n=1-8$): Comparison of density-functional and many-body theories

Murilo L. Tiago,[1] Juan C. Idrobo,[1,2,3] Serdar Öğüt,[2] Julius Jellinek,[4] and James R. Chelikowsky[5]
[1]*Oak Ridge National Laboratory, Oak Ridge, Tennessee 37831, USA*
[2]*Department of Physics, University of Illinois at Chicago, Chicago, Illinois 60607, USA*
[3]*Department of Physics and Astronomy, Vanderbilt University, Nashville, Tennessee 37235, USA*
[4]*Chemical Sciences and Engineering Division, Argonne National Laboratory, Argonne, Illinois 60439, USA*
[5]*Departments of Physics and Chemical Engineering, Center for Computational Materials, Institute for Computational Engineering and Sciences, University of Texas, Austin, Texas 78712, USA*
(Received 17 December 2008; revised manuscript received 17 February 2009; published 13 April 2009)

We analyze the electronic and optical excitations in silver clusters ($Ag_n$, $n=1-8$) using density-functional and many-body theories within an *ab initio* pseudopotential framework. Vertical ionization potentials and electron affinities are calculated within the so-called ΔSCF and *GW* approximations. Results are compared with experimental data. For molecular orbitals of predominantly *sp* character, the *GW* results are found to be in good agreement with experiment. For orbitals of mainly *d* character, good agreement with experiment can be achieved only via the use of semicore pseudopotentials, due to strong correlations among 4*s*, 4*p*, and 4*d* electrons. Optical excitations are computed within the time-dependent local-density approximation (TDLDA) and by solving the Bethe-Salpeter equation (BSE) for electrons and holes. For most clusters, the TDLDA spectra are in reasonable agreement with experimental data. The optical excitations computed with the BSE method, on the other hand, are generally in poor agreement with experiment, especially as size increases. This finding is explained in terms of the nonlocality of the BSE kernel and correlations involving 4*d* electrons. We also discuss the roles played by self-consistency, vertex corrections, and satellite structures in the *GW* results of these confined systems with *d* valence electrons.

DOI: 10.1103/PhysRevB.79.155419 PACS number(s): 78.67.−n, 36.40.Vz, 73.22.−f

## I. INTRODUCTION

During the last decade and a half, dielectric and optical properties of clusters and nanoparticles have received an increasing level of attention from both experimental and theoretical sides. In particular, much progress has been achieved in the implementation and application of various techniques for predicting and understanding optical properties of these confined systems from first principles. Currently, time-dependent density-functional theory (TDDFT) (Refs. 1–3) and a many-body perturbative approach based on the solution of the Bethe-Salpeter equation for the two-particle Green's function,[4–7] the so-called *GW*BSE method, are two of the state-of-the-art computational techniques that are widely used for first-principles computations of the absorption spectra of clusters. The applications of these two techniques have so far focused mainly on *sp*-bonded systems. Nanostructures in which *d* electrons and their screening interactions with *sp* electrons play important roles in the nature of the optical excitations are both scientifically interesting and computationally more challenging, since the inclusion of *d* electrons requires larger basis set sizes. The goal of this paper is to present a comparison of the predictions of the two methods, TDDFT within the adiabatic local-density approximation (TDLDA) and *GW*BSE, when applied to noble-metal clusters of Ag, which have fully occupied valence *d* orbitals.

Although the fundamental equations for TDDFT and *GW*BSE are similar and both formalisms are exact, the predictions from the two formalisms can differ significantly owing to the different approximations made in practical applications. For example, in extended systems, adiabatic TDLDA has been shown to give rather poor results when its predictions are compared with experimental data.[7] In a variety of bulk insulators and semiconductors, *GW*BSE, on the other hand, has captured the essential features of the absorption spectrum, in particular the excitonic effects.[6,7] This failure of the TDLDA in extended systems has been attributed to several factors, in particular, the neglect of dynamical correlations and the absence of long-range interactions between electrons and holes. Three observations indicate that long-range interactions are important in the context of excitonic effects: (1) excitonic effects can be recovered within TDDFT if a nonlocal kernel with the appropriate long-range behavior is employed;[8] (2) the TDLDA has been shown to give rather accurate excitation energies in finite systems such as clusters and isolated atoms;[9–15] and (3) the TDLDA has been shown to predict accurately the optical threshold of the *F* center, a localized vacancy in the LiCl crystal.[13]

Designing universal TDDFT functionals which capture the correct ingredients remains a challenge in the field. This task can only be done after the deficiencies of existing functionals are uncovered and the necessary properties of accurate functionals are identified. In this work, we analyze the importance of correlations involving *d* electrons, which is an important aspect in the broader scenario of functional design. The paper is organized as follows: Sec. II has a brief explanation of the theoretical-computational methodology. Section III has a discussion of the electronic excitations, namely, the ionization potentials and electron affinities of the Ag atom and $Ag_n$($n=2-8$) clusters. Optical excitations of $Ag_n$($n=1-8$) are presented and discussed in Sec. IV. We continue with separate discussions of three aspects related to the

 

TABLE I. Numerical parameters used in the present calculations. The grid spacing ($h$) and the boundary radius ($R_{\max}$) are given in a.u. $N_{\dim}$, $N_s$, and $N_{\mathrm{TDLDA}}$ denote the number of grid points in the real-space mesh (size of the DFT Hamiltonian), the total number of Kohn-Sham orbitals, and the dimension of the TDLDA matrix, respectively. $S$ denotes the computed optical sum-rule ratio, as discussed in the text. $N_{\mathrm{TDLDA}}$ is equal to the product of occupied and empty Kohn-Sham orbitals, with spin degrees of freedom taken into account.

| | $h$ | $R_{\max}$ | $N_{\dim}$ | $N_s$ | $N_{\mathrm{TDLDA}}$ | $S$ (%) |
|---|---|---|---|---|---|---|
| Ag | 0.4 | 24 | 904,960 | 700 | 7639 | 35.6 |
| $Ag_2$ | 0.4 | 24 | 904,960 | 700 | 7579 | 33.6 |
| $Ag_3$ | 0.4 | 24 | 904,960 | 300 | 9355 | 24.9 |
| $Ag_4$ | 0.4 | 24 | 904,960 | 300 | 6116 | 25.0 |
| $Ag_5$ | 0.4 | 24 | 904,960 | 320 | 16,087 | 25.3 |
| $Ag_6$ | 0.45 | 25 | 718,210 | 300 | 8811 | 23.9 |
| $Ag_7$ | 0.45 | 25 | 718,210 | 300 | 20,135 | 23.4 |
| $Ag_8$ | 0.45 | 25 | 718,210 | 300 | 11,264 | 23.2 |

*GW*BSE theory (satellite structure, self-consistency, and vertex corrections) and their implications in the excitation spectra of the clusters studied. We conclude with a brief summary of our findings in Sec. VI.

## II. THEORETICAL BACKGROUND AND COMPUTATIONAL METHODS

### A. Density-functional theory

The many-body ground state of clusters is calculated in the framework of density-functional theory (DFT).[16,17] We use a real-space approach, which allows us to impose the proper boundary conditions in a simple and straightforward manner: the electron wave functions and charge density are required to vanish outside a sphere centered on the cluster.[18,19] Wave functions are calculated directly on a regular mesh of points in real space. Two parameters control numerical accuracy: the radius of the boundary sphere $R_{\max}$ and the grid spacing $h$. The numerical parameters used to obtain the results in this paper are listed in Table I. During the solution of the Kohn-Sham equations, we calculate the Laplacian of wave functions using finite differences of order 12 (six neighbors on each side of a given grid point). We use the exchange-correlation potential in the local-density approximation (LDA).[20,21] The electron-ion interaction is modeled with *ab initio* norm-conserving scalar-relativistic pseudopotentials generated from the reference configuration $4d^{10}5s^{1}5p^{0}$. We solve the Kohn-Sham equations using a Chebyshev-Davidson eigenvalue algorithm, and if an initial set of eigenvalues or eigenvectors is known, by subspace filtering with Chebyshev polynomials.[22] DFT calculations are performed using the PARSEC code.[18,19] The ground-state structures of $Ag_n(n=2-8)$ employed in this study are those obtained in Ref. 23, also shown in Fig. 1 of Ref. 12.

### B. Time-dependent density-functional theory

Being a ground-state theory, DFT does not give direct access to optical excitations. The natural approach within the spirit of DFT is a time-dependent extension. In that approach, an external time-dependent potential is added to the Hamiltonian and the response of the electron density to this potential is calculated. In the limit of very weak external potential, the important quantity is the polarizability $\Pi(1,2)=\frac{\delta\rho(1)}{\delta V_{\mathrm{ext}}(2)}$. Here, we use a many-body notation for space, time and spin variables: $(1)=(\mathbf{r}_1,t_1,\tau_1)$. We assume that the polarizability can be written as a sum over normal modes.[2,11] In frequency domain, the polarizability is

$$\Pi(\mathbf{r},\mathbf{r}';E)=\sum_s \rho_s(\mathbf{r})\rho_s(\mathbf{r}')\left[\frac{1}{E-\omega_s+i0^+}-\frac{1}{E+\omega_s-i0^+}\right], \tag{1}$$

where the frequencies of the normal modes of excitation in the system are denoted by $\omega_s$. $0^+$ represents a positive infinitesimal. We expand $\rho_s$ in a series of single-particle transitions from an occupied orbital $v$ to an unoccupied orbital $c$,

$$\rho_s(\mathbf{r})=\sum_{vc} X^s_{vc}\varphi_v(\mathbf{r})\varphi_c(\mathbf{r})\left(\frac{\varepsilon_c-\varepsilon_v}{\omega_s}\right)^{1/2}, \tag{2}$$

where Kohn-Sham eigenvalues are denoted $\varepsilon_i$, with corresponding eigenfunctions $\varphi_i$. We assume $\hbar=1$ throughout. We also assume that the electronic system is not periodic, so that wave functions $\varphi$ and amplitudes $\rho$ are real quantities. The coefficients $X$ above satisfy Casida's eigenvalue equation,[2]

$$\mathbf{R}^{1/2}[\mathbf{R}+4(\mathbf{K}^x+\mathbf{K}^{xc})]\mathbf{R}^{1/2}\mathbf{X}=\omega_s^2\mathbf{X}, \tag{3}$$

where $\mathbf{R}$, $\mathbf{K}^x$, and $\mathbf{K}^{xc}$ are matrices in the space of single-particle transitions,

$$R_{vcv'c'}=\delta_{vv'}\delta_{cc'}(\varepsilon_c-\varepsilon_v), \tag{4}$$

$$\mathbf{K}^x_{vcv'c'}=\int d\mathbf{r}\int d\mathbf{r}'\,\varphi_v(\mathbf{r})\varphi_c(\mathbf{r})\frac{e^2}{|\mathbf{r}-\mathbf{r}'|}\varphi_{v'}(\mathbf{r}')\varphi_{c'}(\mathbf{r}'), \tag{5}$$

$$\mathbf{K}^{xc}_{vcv'c'} = \int d\mathbf{r}\varphi_v(\mathbf{r})\varphi_c(\mathbf{r})f_{xc}(\mathbf{r})\varphi_{v'}(\mathbf{r})\varphi_{c'}(\mathbf{r}). \quad (6)$$

The generalized eigenvectors $\mathbf{X}$ are orthonormalized, $\mathbf{X}^s\mathbf{X}^{s'} = \delta_{ss'}$.

According to Eqs. (5) and (6), electromagnetic fields in the system are screened by two mechanisms: electrostatic screening produced by valence electrons, and exchange-correlation screening arising from the fact that valence electrons interact among themselves also through quantum-mechanical exchange and correlation. The first mechanism is contained in $\mathbf{K}^x$. The second one is contained in $\mathbf{K}^{xc}$. In the random-phase approximation (RPA), exchange-correlation screening is ignored by setting $\mathbf{K}^{xc}$ to zero.[24,25] In time-dependent DFT, the exchange-correlation kernel is a functional derivative of the exchange-correlation potential, $f_{xc} = \frac{\delta V_{xc}}{\delta \rho}$. Mirroring the Kohn-Sham formulation of DFT, TD-DFT also relies on a known approximation for the exchange-correlation potential $V_{xc}$. In the local-density approximation (TDLDA), $f_{xc}$ becomes local and energy independent.[2,3,7,11]

During the calculation of the polarizability, there are two numerically intensive steps: (I) evaluating the nonlocal integrals in Eq. (5) and (II) diagonalizing the eigenvalue problem in Eq. (3). Assuming that the amplitudes $\rho_s$ are expanded in a total of $N_{\mathrm{TDLDA}}$ pairs of occupied and unoccupied orbitals and that the discretized space has $N_{\mathrm{dim}}$ points, step (I) scales as $[N_{\mathrm{TDLDA}}]^2 \times [N_{\mathrm{dim}}]^2$ in the worst case, namely, when the integral is done by direct summation over grid points. Better scaling is achieved if one computes the integral using Fourier transforms with an appropriate truncation of the Coulomb interaction across images. Owing to the quasilinear scaling of the fast Fourier transform (FFT), the scaling of step (I) reduces to $[N_{\mathrm{TDLDA}}]^2 \times [N_{\mathrm{dim}} \log(N_{\mathrm{dim}})]$.[13,26] Step (II) scales as $[N_{\mathrm{TDLDA}}]^3$ but, having a small prefactor, it is never the most numerically intensive step unless $N_{\mathrm{TDLDA}}$ is very large. In the case of $Ag_n (n \leq 8)$ clusters, step (I) is usually orders of magnitude more intensive than step (II). The dimensions of the TDLDA matrices are listed in Table I. Further simplification is achieved if the cluster has a symmetric geometry with $N_s$ symmetry representations. In that case, portions of the $\mathbf{K}^x$ matrix will vanish by selection rule. Scaling of steps (I) and (II) then reduce to $[N_{\mathrm{TDLDA}}]^2 \times [N_{\mathrm{dim}} \log(N_{\mathrm{dim}})] \times [N_s]^{-2}$ and $[N_{\mathrm{TDLDA}}]^3 \times [N_s]^{-2}$, respectively.

### C. Green's function in the *GW* approximation

An alternative theory for electronic structure is based on computing the electronic Green's function of the system and using it to calculate other response functions. Within the quasiparticle approximation, the Green's function is given in terms of the quasiparticle energies $E_n$ and wave functions $\psi_n$ as

$$G(1,2) = -i\sum_{n=1}^{\infty} g_n \psi_n(\mathbf{r}_1,\tau_1)\psi_n(\mathbf{r}_2,\tau_2) \times \exp[-ig_n E_n(t_1-t_2)]\Theta[g_n(t_1-t_2)], \quad (7)$$

where the parameter $g_n$ is $-1$ for occupied orbitals and 1 for unoccupied orbitals, and $\Theta$ is the step function. When expressed in energy representation, the Green's function above has poles at energies $E_n$, which correspond to peaks in direct and inverse photoemission spectra.

Using Eq. (7) and Dyson's equation, we obtain an eigenvalue equation for the orbitals,

$$\left[\frac{-\nabla^2}{2m} + V_{e-i} + V_H\right]\psi_n(\mathbf{r}) + \int d\mathbf{r}'\Sigma(\mathbf{r},\mathbf{r}',E_n)\psi_n(\mathbf{r}') = E_n\psi(\mathbf{r}), \quad (8)$$

where $V_{e-i}$ is the electron-ion potential (replaced with a pseudopotential in our calculations), $V_H$ is the electrostatic potential created by electrons, and $\Sigma$ is the electron self-energy. The *GW* approximation (*GW*A) is based on expressing the electron self-energy as a power series in the screened Coulomb interaction ($W$) and retaining only the lowest-order terms.[4,27] As a result, the self-energy has an exact expression as the product of Green's function, the screened Coulomb interaction, and the vertex operator: $\Sigma = iGW\Gamma$.

Several levels of approximation have been used to calculate the self-energy, depending on how the quantities $G$, $W$ and $\Gamma$ are calculated. The most basic level is commonly referred to as $G_0W_0$. At that level of approximation, the Green's function is assumed equal to the DFT Green's function, the polarizability is calculated within RPA, and the vertex operator is set to identity. The self-energy is then a product of the Green's function and the screened Coulomb interaction,

$$\Sigma(1,2) = iG_0(1,2)W_0(2,1^+) = iG_0(1,2)V(2,1^+) + iG_0(1,2)\int d(3,4)V(2,3)\Pi_0(3,4)V(4,1^+), \quad (9)$$

where $\Pi_0$ is the RPA polarizability. Subscript in $G_0$ indicates that DFT eigenfunctions and eigenvalues are used to calculate the Green's function. The first term on the right-hand side of Eq. (9) corresponds to Fock (exact) exchange in the Kohn-Sham system. It assumes a more familiar form when we write the space/time/spin indices explicitly,

$$iG_0(1,2)V(2,1^+) = -\sum_{n}^{occ.} \varphi_n(\mathbf{r}_1,\tau_1)\varphi_n(\mathbf{r}_2,\tau_2)\frac{e^2}{|\mathbf{r}_1-\mathbf{r}_2|}\delta(t_1-t_2). \quad (10)$$

The second term in Eq. (9) contains quantum-mechanical correlations, included in the polarizability.

At a higher level of approximation, vertex corrections can be added to Eq. (9). Assuming that the LDA gives a good approximation to $\Sigma$ and $G$ in the exact integrodifferential satisfied by the vertex operator,[27] we can obtain the following approximate form for $\Gamma$:

$$\Gamma(1,2;3) \approx \delta(1,2)\delta(1,3) - i\delta(1,2)f_{xc}(1)\int d(4,5)G(1,4)G(5,1^+)\Gamma(4,5,;3), \tag{11}$$

where $f_{xc}$ is the LDA kernel.[13,28,29] Using Eq. (11) amounts to modifying Eq. (9) in two ways: first, vertex-related terms are explicitly added to Eq. (9), and second, the RPA polarizability is replaced with a polarizability calculated within TDLDA. These modifications lead to the $G_0W_f$ approximation,

$$\Sigma(1,2) = iG_0(1,2)V(2,1^+) + iG_0(1,2)\int d(3,4)V(2,3)\Pi_f(3,4)V(4,1^+) + \frac{i}{2}G_0(1,2)\int d(3)[V(2,3)\Pi_f(3,1^+)f(1^+) + f(2)\Pi_f(2,3)V(3,1^+)], \tag{12}$$

where Fock exchange is kept and correlation has a more generic form. $\Pi_f$ denotes the TDLDA polarizability. Unless otherwise stated, we employ the $G_0W_f$ approximation in the subsequent discussion. Most of the small clusters have point symmetries. We incorporate point symmetries explicitly in the self-energy by classifying polarizability poles according to their point-group representation. More details can be found in the literature.[4,13]

Accurate calculations of the self-energy for clusters are challenging because they involve correlations between occupied orbitals and unoccupied ones at much higher energies. This means that the Green's function in Eqs. (9) or (12) should be evaluated with a very large number of orbitals. The convergence of the sum over $n$ in Eq. (7) is usually slow.[4,30] We accelerate this convergence by including a *static remainder* as proposed in Ref. 13. The justification behind the static remainder is that correlations involving high-energy virtual orbitals are not specific to the $G_0W_0$ or $G_0W_f$ approximations. They also exist in the static or the Coulomb-hole-screened-exchange (COHSEX) approximation.[4,5,27] Moreover, the rate at which these correlations decay as the energy of virtual orbitals increase is similar for all those approximations. One can then estimate the numerical error by truncating the summation over virtual orbitals at the level of the COHSEX approximation and transfer that estimate, the static remainder, to more accurate approximations. We have tested the usefulness and reliability of the static remainder in some of the clusters investigated here, and found that it significantly improves the convergence of calculations with respect to the number of orbitals included. We will return to this issue in Sec. III.

Since we express the polarizability in energy representation, its energy dependence around the plasma frequency (typically ~5–20 eV) must be known. This behavior contrasts with the calculation of TDLDA optical spectra,[12] for which the convergence up to a given energy $E$ can be achieved by including excitations in a narrower frequency range around $E$, which is typically no more than a few eVs. We handle this convergence issue by including a large number of unoccupied Kohn-Sham orbitals. We monitor the convergence of polarizability poles through the optical sum-rule ratio, $S$, which is defined as the ratio between the polarizability numerically integrated in energy and its exact value, given by the so-called $f$-sum rule.[4] Values of the numerical parameters for the clusters studied are reported in Table I. We note that we have performed extensive convergence tests for TDLDA and $GW$BSE results by increasing the radius of the boundary sphere $R_{\max}$ from 24 up to 36 a.u. for the atom and the dimer and to 30 a.u. for $n \geq 3$. In addition, we tested the convergence with respect to the number of unoccupied orbitals. From these tests, we conclude that $GW$ results are converged within less than 0.1 eV and both the TDLDA and $GW$BSE optical spectra are converged up to energies ~5.5–6 eV.

Within the $GW$A, the ionization potential (IP) is the negative of the quasiparticle energy of the highest occupied molecular orbital (HOMO). In $Ag_n$ clusters with an even number of electrons, this orbital is spin degenerate. In clusters with an odd number of electrons, the HOMO is nondegenerate and completely filled with an unpaired electron. The electron affinity (EA) is the negative of the quasiparticle energy of the lowest unoccupied molecular orbital (LUMO), which can also be degenerate or not depending on the parity of the cluster. In the present study, we calculate the quasiparticle energies by diagonalizing Eq. (8) using the self-energy obtained within the $G_0W_f$ approximation.

### D. Many-body neutral excitations: Bethe-Salpeter equation

In a many-electron system, the polarizability is related to the electron-hole Green's function[6,25] as $\Pi(1,2) = -iL(1,2;1^+,2^+)$. In energy representation, both quantities can be expressed as sums over poles, for example,

$$\Pi(\mathbf{r},\mathbf{r}',E) = \sum_s \chi_s(\mathbf{r})\chi_s(\mathbf{r}')\left[\frac{1}{E-\Omega_s+i0^+} - \frac{1}{E+\Omega_s-i0^+}\right]. \tag{13}$$

The amplitudes $\chi_s$ describe the probability of creating one uncorrelated electron-hole pair in the ground state of the system and reaching excited state $s$. In the Tamm-Dancoff approximation, we assume that electrons and holes can be created only on unoccupied and occupied quasiparticle orbitals, respectively.[25] Therefore, the amplitudes $\chi$ can be expanded in terms of products between occupied and unoccupied quasiparticle orbitals,

$$\chi_s(\mathbf{r}) = \sum_{vc} A^s_{vc}\psi_v(\mathbf{r})\psi_c(\mathbf{r}). \tag{14}$$

The coefficients $A_{vc}$ satisfy an eigenvalue equation known as Bethe-Salpeter equation (BSE). In matrix form and assuming static screening, the BSE is

$$[\mathbf{D} + 2(\mathbf{K}^x + \mathbf{K}^d)]\mathbf{A} = \Omega_s\mathbf{A}. \tag{15}$$

Matrix $\mathbf{D}$ is a difference between quasiparticle eigenvalues, $\mathbf{D}_{vcv'c'} = \delta_{vv'}\delta_{cc'}(E_c - E_v)$. The so-called "direct kernel" $\mathbf{K}^d$ is a functional derivative of the self-energy,

TABLE II. Vertical ionization potentials and electron affinities of $Ag_n(n \leq 8)$ computed with *GW* theory and ΔSCF method along with the experimental estimates (Refs. 31–33). The values for the singly ionized Ag atom in the last row are computed using a pseudopotential which includes 4*s* and 4*p* semicore states, as discussed in the text. All energies are in eV.

| | Ionization potential (eV) | | | Electron affinity (eV) | | |
|---|---|---|---|---|---|---|
| Cluster | Expt.[a] | ΔSCF | *GW* | Expt.[b] | ΔSCF | *GW* |
| Ag | 7.57 | 8.23 | 7.53 | 1.30 | 1.60 | 1.26 |
| $Ag_2$ | 7.60 | 8.37 | 7.54 | 1.06 | 1.21 | 1.12 |
| $Ag_3$ | 6.20 (5.66) | 6.34 | 5.84 | 2.43 | 2.67 | 2.76 |
| $Ag_4$ | 6.65 | 6.99 | 6.49 | 1.65 | 1.89 | 1.83 |
| $Ag_5$ | 6.35 (5.74) | 6.59 | 6.02 | 2.11 | 2.36 | 2.33 |
| $Ag_6$ | 7.15 | 7.45 | 6.80 | 2.06 | 1.62 | 1.58 |
| $Ag_7$ | 6.40 (5.69) | 6.37 | 5.72 | 2.55 | 2.26 | 2.20 |
| $Ag_8$ | 7.10 | 7.27 | 6.48 | 1.65 | 1.43 | 1.44 |
| $Ag^+$ | 21.5 | 22.1 | 18.92 | 7.57 | 8.23 | 7.64 |
| $Ag^+$ (semicore psp) | 21.5 | 22.2 | 21.85 | 7.57 | 8.41 | 7.30 |

[a]From Reference 31. The values in parentheses for $n=3,5$, and 7 are from Reference 32.
[b]From Reference 33.

$\mathbf{K}^d(1,2;3,4)=\frac{\delta\Sigma(1,3)}{\delta G(4,2)}$. In the space of single-particle transitions, the kernel can be expressed as

$$\mathbf{K}^d_{vcv'c'} = \int d\mathbf{r} \int d\mathbf{r}' \psi_v(\mathbf{r})\psi_{v'}(\mathbf{r}) \left[ \frac{e^2}{|\mathbf{r}-\mathbf{r}'|} + W'(\mathbf{r},\mathbf{r}') \right] \psi_c(\mathbf{r}')\psi_{c'}(\mathbf{r}'), \quad (16)$$

with

$$W'(\mathbf{r},\mathbf{r}') = -\int d\mathbf{r}''d\mathbf{r}''' \left\{ \frac{e^2}{|\mathbf{r}-\mathbf{r}''|} \Pi_f(\mathbf{r}'',\mathbf{r}''';0) \frac{e^2}{|\mathbf{r}'''-\mathbf{r}'|} \right\} - \frac{1}{2}\int d\mathbf{r}'' \left\{ \frac{e^2}{|\mathbf{r}-\mathbf{r}''|} \Pi_f(\mathbf{r}'',\mathbf{r}';0) f_{xc}(\mathbf{r}') \right\} - \frac{1}{2}\int d\mathbf{r}'' \left\{ f_{xc}(\mathbf{r}) \Pi_f(\mathbf{r},\mathbf{r}'';0) \frac{e^2}{|\mathbf{r}''-\mathbf{r}'|} \right\}. \quad (17)$$

There are striking similarities between the TDDFT formulation of polarizability from Sec. II B and the present many-body formulation.[7] In both formulations, the polarizability is determined by fluctuation amplitudes that are products of Kohn-Sham eigenfunctions (TDDFT) or products of quasiparticle wave functions (BSE). Also, the amplitudes are determined by eigenvalue problems: Eq. (3) for TDDFT or Eq. (15) for BSE. Finally, both eigenvalue problems have exchange-correlation screening: $K^{xc}=\frac{\delta V_{xc}}{\delta \rho}$ (TDDFT) or $K^d=\frac{\delta\Sigma}{\delta G}$ (BSE).

The scaling of numerical complexity in the BSE with respect to system size is similar to TDDFT (scaling approximately as the fifth power in the number of atoms in the cluster). The computations of the self-energy and the direct kernel $\mathbf{K}^d$ are both dominated by integrals of the form of Eq. (5). However, the prefactor in the *GW*BSE method is much larger than that in TDDFT, since the polarizabilities $\Pi_0$ or $\Pi_f$ need to be computed in advance for a *GW*BSE calculation.

## III. ELECTRONIC EXCITATIONS IN SILVER CLUSTERS

Table II shows the vertical ionization potentials and electron affinities of $Ag_n$, $n=1-8$, along with the experimental estimates. The calculated vertical IP is the lowest energy required to remove one electron from the cluster, assuming that the nuclei do not move to a lower energy configuration during the ionization process. Most of the experimental estimates for IPs listed in Table II come from an electron-impact ionization study by Jackschath *et al.*[31] These experimental values were reported as the upper limits for the vertical IPs with an error bar of ~0.1 eV in this size range. We also list the values obtained in another set of experiments by Alameddin *et al.*[32] for $n=3$, 5, and 7, which are significantly lower than those in the previous set (by as much as 0.7 eV). Similarly, the calculated vertical EA is the energy released by the neutral cluster when an extra electron binds to it in the absence of atomic relaxation. The experimental estimates for EAs listed in Table II from a photoelectron spectroscopy study of cluster anions by Ho *et al.*[33] are actually the measured vertical detachment energies (VDEs) defined as the electron binding energies at the peaks of the lowest electronic transitions. The measured values are generally in good agreement with other experimental estimates in the literature.[34,35] In our comparisons of the calculated values with experimental data, we assume (with the exception of the case for $Ag_3$, please see below) that the geometries of the neutral clusters and the cluster anions are similar, and that the experimental VDEs, which are more directly comparable to vertical EAs at the geometry of the cluster anions, give a reasonable estimate for the vertical EAs at the geometry of the neutral clusters.

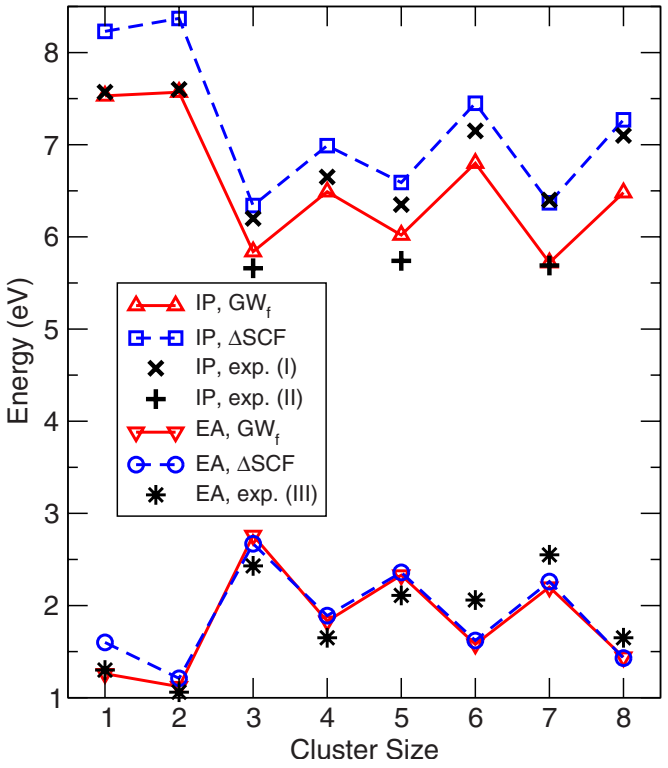


FIG. 1. (Color online) $G_0W_f$ ionization potentials (red continuous line with △ signs), ΔSCF ionization potentials (blue dashed line with □ signs), experimental ionization potentials (black crosses and plus signs), $G_0W_f$ electron affinities (red continuous line with ▽ signs), ΔSCF electron affinities (blue dashed line with circles), and experimental electron affinities (black stars) as a function of size for $Ag_n(n=1-8)$. Three sets of experimental data are reported: Experimental ionization potential (i) in black crosses from Ref. 31, (ii) in black plus signs from Ref. 32, and (iii) in black stars from Ref. 33.

In our study, the vertical IPs and EAs were first calculated at the DFT level, by computing the difference in DFT total energies between the charged cluster and the neutral cluster. This is the so-called ΔSCF method.[36] As shown in Table II (also displayed in Fig. 1), IPs obtained with the ΔSCF method are typically larger than the experimental estimates by up to 0.77 eV depending on the size. The ΔSCF electron affinities, on the other hand, can be smaller by as much as 0.44 eV ($Ag_6$) or larger by 0.30 eV (Ag atom) than the experimental estimates. We note that for $Ag_3$, the EA values reported in Table II for both the ΔSCF and *GW* methods are obtained by performing the calculations at the geometry of the anion, which is a symmetric linear molecule (with a nearest-neighbor distance of 2.66 Å). The EA calculations performed at the isosceles triangle geometry of the neutral cluster result in ΔSCF and *GW* values of 1.65 and 1.69 eV, respectively, which are much smaller than the experimental value of 2.43 eV. The IP and EA values calculated with the ΔSCF method are converged with respect to the computational parameters ($R_{max}$ and $h$) to within 0.01 eV. The discrepancies between experiment and ΔSCF can, therefore, be attributed to possible structural changes upon charging, the possibility of different isomers, the spurious self-interaction effects, or the inadequacy of the LDA due to the incorrect asymptotic behavior. Given that the first two reasons are not valid for the Ag atom, for which the largest deviations in IP and EA are observed, LDA and/or the self-interaction effects are the most likely reasons for the observed discrepancies.

TABLE III. The effect of the static remainder correction in the calculated vertical ionization potentials and electron affinities of $Ag_n(n\leq 8)$. The $G_0W_f$ approximation is used in the self-energy. The values under the columns marked with "NS" do not include the static remainder, while the values under the column "ST" do. All energies are in eV.

| | Ionization potential (eV) | | Electron affinity (eV) | |
|---|---|---|---|---|
| Cluster | NS | ST | NS | ST |
| Ag | 7.12 | 7.53 | 0.92 | 1.26 |
| $Ag_2$ | 6.27 | 7.54 | 0.82 | 1.12 |
| $Ag_3$ | 5.19 | 5.84 | 2.20 | 2.76 |
| $Ag_4$ | 5.56 | 6.49 | 1.14 | 1.83 |
| $Ag_5$ | 5.04 | 6.02 | 1.78 | 2.33 |
| $Ag_6$ | 5.18 | 6.80 | 1.06 | 1.58 |
| $Ag_7$ | 4.70 | 5.72 | 1.61 | 2.20 |
| $Ag_8$ | 5.10 | 6.48 | 0.94 | 1.44 |
| $Ag^+$ | 16.64 | 18.92 | 7.34 | 7.64 |
| $Ag^+$ (semi-core psp) | 20.67 | 21.85 | 7.04 | 7.30 |

Next, we calculated the vertical ionization potentials and electron affinities for $Ag_n$ within the *GW*A. We first compare *GW* and ΔSCF results with each other (cf. Fig. 1) and observe two trends: (i) the predictions for the IPs from the ΔSCF method are consistently higher than those from the *GW*A by an average of ~0.65 eV. (ii) The predictions from *GW* and ΔSCF for the EAs, on the other hand, are quite close, within less than 0.1 eV of each other (with the exception of the Ag atom). These trends are similar in nature, but decidedly different compared to those observed in other confined systems. For example, for hydrogenated Si quantum dots (up to ~1.7 nm in diameter), Tiago and Chelikowsky have also shown that *GW* and ΔSCF EAs are very close (within 0.1 eV) of each other, while there is a systematic discrepancy between the IPs calculated with the two approaches.[13] However, unlike the trend observed in $Ag_n$ clusters, in $Si_nH_m$ quantum dots it is the IPs calculated within the *GW*A that are systematically higher by 0.6 to 0.9 eV than those calculated with the ΔSCF method.

Self-energies are very sensitive to the number of orbitals used to compute the Green's function in Eq. (7). This behavior has been reported several times and several methods have been proposed to address this issue.[13,30] As mentioned in Sec. II C, in the present study we add a static remainder correction from the COHSEX approximation.[13] We have done exhaustive convergence tests with respect to the number of orbitals and observed that the static remainder indeed accelerates convergence of both IP and EA. Table III shows that, for a given cluster, the static remainder correction for the IP is not equal to the static remainder correction for the EA. In other words, the electronic gap is also affected by the slow convergence of self-energy with respect to the number of

Kohn-Sham orbitals. An underconverged calculation of quasiparticle energies would result in incorrect excitation energies and incorrect optical spectra.

Given the systematic and significant differences between the IPs calculated with ΔSCF and *GW* methods, it is natural to ask which of the two approaches is more accurate when their predictions are compared with experimental data on $Ag_n$ ($n=1-8$). For sizes $n \geq 3$, the comparison with experimental IP values is complicated by the fact that the two sets of existing experimental data ($n=1-8$ in Ref. 31 and $n=3,5,7$ in Ref. 32) differ from each other by as much as 0.7 eV. For sizes $n=3$, 5, and 7, the IPs calculated from the *GW* theory are in good agreement with experimental data in Ref. 32, while the IPs calculated within ΔSCF for the same sizes have a good agreement with experimental data in Ref. 31. The large differences in the two sets of experimental values make it difficult to present a more conclusive comparison among *GW*, ΔSCF and experimental data. However, two observations about the comparison of experimental and theoretical results suggest that the *GW* theory is more accurate for the calculation of IPs in $Ag_n$ clusters. First, as shown in Fig. 1, the IPs calculated within *GW* theory are all smaller than the experimental results of Jackschath *et al.*[31] This trend in *GW* values, not observed in ΔSCF results, is consistent with the expectation that the reported experimental values should provide an upper bound for the true vertical IPs. Second and more importantly, focusing on the smallest sizes, Ag and $Ag_2$, for which the most reliable experimental data exist, we see that *GW* method is far more accurate than the ΔSCF method. Both the IP and EA predictions from the *GW* theory for Ag and $Ag_2$ are excellent, typically within 0.05 eV of the experimental data.

The overall good agreement of the *GW* results with experimental data is encouraging. However, our analysis shows that the observed agreement at this level of theory is due to the fact that the HOMO and LUMO of $Ag_n (n \leq 8)$ clusters have almost entirely *sp* orbital character with no or very little *d* contribution. For example, the HOMO of $Ag_2$ has almost entirely *s* character with ~8% *d* character, and its LUMO has *s*, *p*, and *d* characters of ~81%, 17%, and 2%, respectively. In order to test how the present *GW* theory works for a system in which HOMO has a large *d* character, we considered the case of the singly ionized silver atom, $Ag^+$, which has a fivefold degenerate HOMO of purely *d* character and a LUMO of purely *s* character. Furthermore, the IP of $Ag^+$ is the double-ionization potential of the Ag atom, which is experimentally available, and the "EA" of $Ag^+$ is simply the IP of the *neutral* Ag atom. The results for IP and EA calculated within the ΔSCF and *GW* theory are presented in Table II. ΔSCF method gives a value of 22.1 eV for the IP of $Ag^+$, compared to the experimental value of 21.5 eV. The magnitude of this overestimate within ΔSCF is very similar to the corresponding value calculated for the neutral atom. The IP calculated with *GW* method, on the other hand, is only 18.92 eV, which is 2.6 eV below the experimental value, indicating that the present method does not adequately describe electronic excitations involving *d* electrons. The "EA" of $Ag^+$ (the IP of neutral Ag) is well described with the present *GW* theory (within less than 0.1 eV of the experimental value), which is not surprising, since the corresponding electronic excitation in that case involves a LUMO of purely *s* character.

The source of error regarding 4*d* electrons goes back to how interactions between them and core electrons are described. During the construction of pseudopotentials, a decision is made about which electrons constitute the core. In general, all electrons that do not participate actively in chemical bonding are lumped in the core.[37] In most constructions of pseudopotentials, exchange-correlation interactions between core and valence electrons are calculated within a simple approximation such as the LDA. In a pseudopotential *GW* calculation, those core-valence interactions are still kept at the LDA level, while exchange-correlation interactions among valence electrons only are described within a many-body theory, which is more refined than DFT. This approach is clearly inadequate if valence electrons are strongly correlated with core electrons.

A DFT-LDA calculation of the silver atom reveals that 4*s* and 4*p* orbitals are, respectively, ~80 and 50 eV lower in energy than the 4*d* orbital. In spite of this large energy separation, the 4*s* and 4*p* orbitals have significant spatial overlaps with 4*d* orbitals. The wave functions of all these orbitals have their outermost radial maxima at around 0.5 Å from the nucleus. In contrast, the outer maximum of the atomic 5*s* orbital occurs at approximately 1.3 Å. Owing to the strong overlap, the exchange interaction among 4*s*, 4*p*, and 4*d* electrons is not described correctly within a Slater exchange as prescribed by the LDA.[21] We have confirmed this deficiency of the LDA by computing the exchange energy of orbital 4*d* in two ways: (I) as a sum of the Fock exchange, Eq. (10), involving orbitals in the shell $[4s,4p,4d]$ plus the Slater (LDA) exchange involving deeper orbitals; and (II) simply as the Slater exchange involving orbital 4*d* and the "large core" that includes 4*p* and 4*s*. The exchange using method (I) is lower than the exchange using method (II) by 4.5 eV. Correlation is also incorrectly described. If not corrected, those errors remain in the self-energy calculation.

A similar problem regarding localized *d* states was addressed more than a decade ago by Rohlfing *et al.*[38,39] in their investigation of the quasiparticle band structure of CdS. In particular, the authors noticed that the *GW* results could be significantly improved to obtain agreement with experiment, if the complete *N*-shell (of principal quantum number 4) of Cd is included in the pseudopotential and the self-energy. Their reasoning indicates that exchange-correlation effects among 4*s*, 4*p*, and 4*d* electrons should be calculated explicitly, preferably at the *GW* level, even if some of those electrons do not contribute to chemical bonding. Alternatively, one can keep the semicore orbitals (4*s* and 4*p*) in the core but include proper exchange and correlation involving them. An example is to include exchange through the exact Fock operator, and correlation with *ad-hoc* methods such as the core-polarization model.[40–42]

Motivated by this observation, we constructed a new Ag pseudopotential including 4*s* and 4*p* orbitals in the valence from the reference configuration $4s^2 4p^6 4d^{10}$ of the singly ionized Ag atom with core radii of 1.1, 1.2, and 2.35 a.u. for *s*, *p*, and *d* orbitals, respectively. We note that the resulting pseudopotentials are quite deep, making it necessary to use a grid spacing of $h=0.2$ a.u. Since this increases the Hamil-

tonian size by almost an order of magnitude, we performed a limited amount of new computations with this pseudopotential focusing mainly on $Ag^+$. The results for IP and EA of $Ag^+$ using the semicore pseudopotential are reported in Table II. The IP within ΔSCF (22.2 eV) is essentially the same as the value computed before with the $(4d,5s,5p)$ pseudopotential. However, the new IP of 21.85 eV calculated within the *GW*A is in much better agreement with the experimental value. The change in IP, from 18.92 to 21.85 eV is less than the error in exchange (4.5 eV) because correlation within the $(4s,4p,4d)$ shell is also strong and of sign opposite to exchange. As a result, they partially cancel each other. In agreement with the findings of Rohlfing *et al.*,[38,39] this result shows that semicore states of the same principal quantum number as the standard valence state need to be included in *GW* calculations for an adequate description of the associated electronic excitations.

The EA of $Ag^+$ (IP of neutral Ag) calculated with the semicore pseudopotential, on the other hand, is now 7.30 eV, somewhat worse compared to the earlier results obtained with the $(4d,5s,5p)$ pseudopotential. In fact, in our tests for the neutral Ag atom and $Ag_2$ cluster, we observed that the IPs and EAs computed with the semicore pseudopotential were not in as good agreement with experiment (typically off by 0.2–0.3 eV) as the previous values obtained with the $(4d,5s,5p)$ pseudopotential (typically within 0.05 eV of experiment). The reason for this is the slight deterioration in the transferability of the semicore pseudopotential. Namely, since our semicore pseudopotential was created from a singly ionized reference configuration, which matches the 4*s*, 4*p*, and 4*d* eigenvalues to the all-electron values and enhances scattering properties around those reference energies, the 5*s* and 5*p* eigenvalues (corresponding to excited states of the semicore pseudopotential) are not expected to be as accurate. Since the IPs and EAs of neutral Ag, $Ag_2$, and the EA of $Ag^+$ all correspond to states of purely or largely 5*s* character, the corresponding results (related to orbitals of largely 5*s* and 5*p* character) obtained with the semicore pseudopotential are not in very good agreement with experimental data. The worsening in the EA of $Ag^+$ within ΔSCF theory (from 8.23 to 8.41 eV, as shown in Table II) also has the same origin. While generating multireference pseudopotentials or using multiple projectors for enhancing scattering properties at higher energies could potentially yield highly transferable semicore pseudopotentials, these will also result in hard pseudopotentials,[43] making it necessary to use very small grid spacings. In summary, these observations suggest that accurate *GW* calculations for $Ag_n$ clusters require highly transferable semicore (or multireference) pseudopotentials for adequate descriptions of quasiparticle states associated with both *d* and *sp* orbitals, which increases the computational demand quite significantly.

## IV. OPTICAL EXCITATIONS OF SILVER CLUSTERS

Neutral optical excitations were computed within two first-principles approaches: the TDLDA and the many-body Bethe-Salpeter method. Figure 2 shows the computed spectra for $Ag_n(n=1-8)$ along with available experimental spectra.[15,44,45] Choices of numerical parameters (Table I)

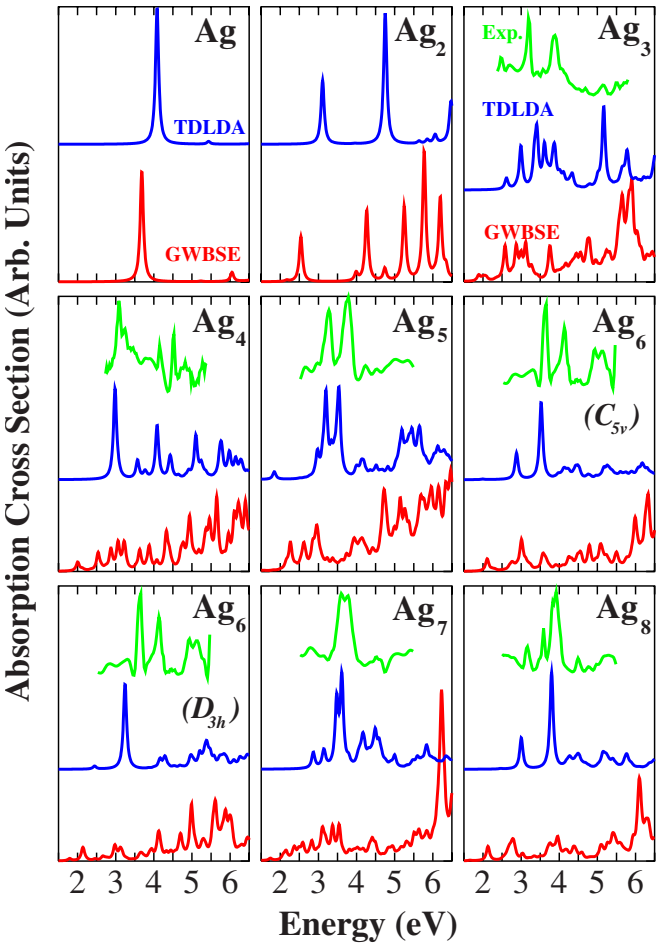


FIG. 2. (Color online) Computed TDLDA (blue curves) and *GW*BSE (red curves) spectra (for $n=1-8$) and experimental (green curves) spectra (for $n=3-8$) of $Ag_n$ clusters as a function of energy. The experimental spectra for $Ag_n$ clusters embedded in Ar matrices are from Refs. 15, 44, and 45. For $Ag_6$, the spectra have been computed for two isomers, the planar ground-state structure of $D_{3h}$ symmetry and the higher-energy three-dimensional isomer (a capped regular pentagon) of $C_{5v}$ symmetry.

were suitable for the oscillator strengths and excitation energies to be converged up to 6 eV. We again used a pseudopotential without explicit semicore orbitals. An overall comparison of the *GW*BSE and TDLDA spectra in Fig. 2 shows the strikingly poor agreement between the two. The disagreement is observed for both the positions and the intensities of the computed peaks. In particular, TDLDA spectra are typically composed of sharp transitions (of large oscillator strength) at low energies (<4–4.5 eV) followed by broader features at higher energies. *GW*BSE, on the other hand, predicts low-energy transitions which are generally redshifted and significantly quenched, and higher-energy transitions which are considerably enhanced with respect to those of TDLDA. Before we examine the possible reasons behind these general observations, we first discuss which of the two theories tends to predict optical excitations in better agreement with available experimental data.

For the Ag atom, the predictions from TDLDA and *GW*BSE for the $5s \rightarrow 5p$ excitation energy are 4.09 and 3.68

eV with corresponding oscillator strengths of $f=0.62$ and 0.51, respectively. The *GW*BSE excitation energy is clearly in better agreement with the experimental value of 3.74 eV, which is obtained by taking the weighted average of $j=1/2$ and $j=3/2$ spin-orbit split transitions measured at 3.66 and 3.78 eV, respectively. The experimental estimate for the oscillator strength is $f=0.7$. The next allowed excitation corresponds to the $5s\rightarrow 6p$ transition measured experimentally at the averaged value of 6.005 eV. The corresponding TDLDA and *GW*BSE transitions are predicted at 5.44 and 6.05 eV, respectively, which again shows that *GW*BSE yields significantly better $s\rightarrow p$ optical excitation energies compared to TDLDA for the case of the Ag atom.

For $Ag_2$, the TDLDA predictions for the most intense low-energy transitions are at 3.11 eV ($f=0.33$) and 4.75 eV ($f=0.67$). These differ significantly from the corresponding *GW*BSE predictions at 2.54 eV ($f=0.23$) and 4.27 eV ($f=0.37$), respectively. We have associated these computed transitions with the experimentally measured $A-X$ and $C-X$ systems[46] at 2.85 and 4.67 eV. As for the experimental $B-X$ system measured at 4.44 eV, we suggest that they are associated with the very low-intensity excitations originating from molecular orbitals of 4*d* character and computed at 3.96 eV (TDLDA) and 3.99 eV (*GW*BSE). Assuming these assignments are valid, it is not clear if TDLDA or *GW*BSE is in better agreement with experimental data, although the $C-X$ data seem to suggest that TDLDA has a slightly better agreement with experiment.

While *GW*BSE results seem to be in good and reasonable agreement for the lowest-energy peaks of Ag and $Ag_2$, respectively, the picture changes considerably for the rest of the clusters. As shown in Fig. 2, for $Ag_n(n\geq 3)$, the *GW*BSE spectra do not even capture the essential features observed in the experiments. On the other hand, the spectra computed within TDLDA have reasonable agreement with experimental data (particularly for $Ag_4$, $Ag_5$, and $Ag_7$), especially if one takes into account that the experiments are performed on clusters embedded in Ar matrices, which could change the positions and intensities of the measured peaks to some degree.[14,15,44] For $Ag_6$, the experimental data, which became available only recently,[45] seem to have a much better agreement with the TDLDA spectrum of the higher-energy isomer of $C_{5v}$ symmetry (a capped regular pentagon), compared to that of the ground-state structure of $D_{3h}$ symmetry (planar geometry). This result is in good agreement with the recent TDDFT studies of Harb *et al.*[15] for the two structures. For $Ag_8$, while the two experimental peaks at 3.16 and 3.91 eV are reproduced well in the TDLDA spectrum of the computed ground-state structure with $T_d$ symmetry, the extra peak in between them at 3.58 eV is not. Recently, Harb *et al.*[15] attributed this peak to a low-energy isomer with $D_{2d}$ symmetry, reproducing the experimental spectrum quite well with a linear superposition of two TDDFT spectra computed for the two different structures. Finally, we note, as discussed in detail in Ref. 12, that our TDLDA results are in very good agreement with those of Yabana and Bertsch in their TDLDA study of $Ag_n$ ($n=1-3,8,9$) clusters.[10]

The analysis so far shows that while the *GW* results for electronic excitations in $Ag_n$ seem to be in good agreement with experimental data for all sizes considered, the BSE results for optical excitations, when compared with experiment and TDLDA results, start to deteriorate as $n\geq 3$. This observation suggests that exchange-correlation effects involving 4*d* orbitals and the strong nonlocality of the *GW*BSE kernel play important roles in the optical spectra as follows: at the Kohn-Sham level, the HOMO and LUMO have predominantly *s* or *sp* characters for all sizes with no or little *d* contribution. Also, the self-energy calculated in the basis of Kohn-Sham wave functions is almost a diagonal matrix, which results in almost 100% overlaps between *GW* and Kohn-Sham wave functions for HOMO and LUMO. The BSE matrix, on the other hand, is strongly nonlocal, mixing *GW* wave functions of *sp* and *d* characters. When the *GW* wave functions of mostly *d* character are not described properly (via the use of a standard pseudopotential, as discussed earlier), the associated optical transitions are not accurately predicted. The problem is actually more severe than one which affects orbitals of predominantly *d* character. Even a small ($\sim$10%) *d* character in the Kohn-Sham or *GW* wave functions results in significant quenching and redshifting of the predicted transitions at the *GW*BSE level. This observation is best illustrated by examining the case for $Ag_2$. Due to the large separation in the energies of the 4*d* and 5*s* atomic orbitals, in $Ag_2$ the atomic *d* orbitals hybridize among themselves, almost completely decoupled from the atomic *s* orbitals. As a result, the first ten doubly occupied (due to spin degeneracy) Kohn-Sham levels in $Ag_2$ have almost purely *d* character. The HOMO and LUMO are almost purely bonding and antibonding combinations of 5*s* atomic orbitals, and the fourfold degenerate LUMO+1 has 5*p* character. The calculated *s*, *p*, and *d* projections of these levels are given in Fig. 3.

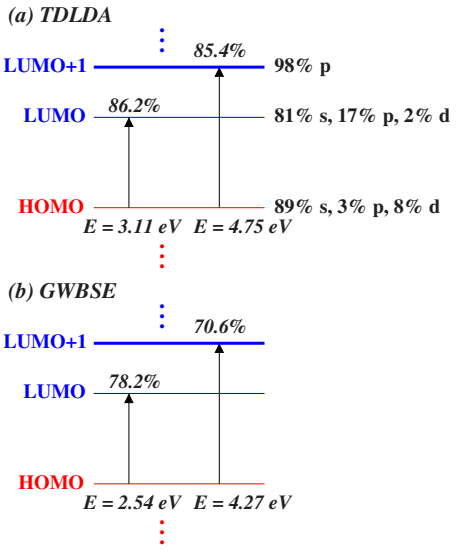


FIG. 3. (Color online) The weights of HOMO→LUMO and HOMO→LUMO+1 transitions in the eigenvectors of the excitations computed for $Ag_2$ at (a) 3.11 and 4.75 eV (within TDLDA), and (b) 2.54 and 4.27 eV (within *GW*BSE). The *s*, *p*, and *d* orbital projections of the Kohn-Sham HOMO and LUMO levels are also provided (see the text for details).

The TDLDA excitation calculated at 3.11 eV is associated primarily with a transition from HOMO to LUMO. The

weight of this transition in the computed TDLDA eigenvector is 86%, by which we mean $|X_{vc}|^2=0.86$ for this particular transition when $v$=HOMO and $c$=LUMO with $X$ defined in Eqs. (2) and (3). Similarly, the TDLDA excitation calculated at 4.75 eV is associated primarily with a transition from HOMO to LUMO+1 with 85% weight in the associated eigenvector. As shown in Fig. 3, while the corresponding *GW*BSE excitations at 2.54 and 4.27 eV are also mainly associated with HOMO→LUMO and HOMO→LUMO+1 transitions, respectively, the weights of these transitions in the computed BSE eigenvectors [as given by $|A_{vc}|^2$ defined in Eq. (14)], 78% and 71%, are considerably smaller than the corresponding TDLDA values. These reductions in HOMO →LUMO and HOMO→LUMO+1 transition weights are obviously compensated by the increase in weights of other transitions involving molecular orbitals derived from atomic 4*d* states. For example, for the excitations computed at 3.11 eV (TDLDA) and 2.54 eV (*GW*BSE), we obtain the following sums when $v$ is restricted to the 4*d* manifold ($v$ =1–10) and $c$ runs from a range of orbitals indexed with $c$ =12 (LUMO) to $c$=40,

$$\sum_{v=1}^{10}\sum_{c=12}^{40}|X_{vc}|^2=0.076(\text{TDLDA}),$$

$$\sum_{v=1}^{10}\sum_{c=12}^{40}|A_{vc}|^2=0.193(\text{GWBSE}). \quad (18)$$

The increase in the *d* character of the optical excitations computed at the *GW*BSE level is accompanied by a redshift in the excitation energies and significant quenching of the oscillator strengths with respect to those at the TDLDA level. In order to capture this effect, we performed a computational thought experiment by "removing" the 4*d* orbitals and recomputing the spectra at both levels of theory. In particular, we zeroed out all components of the kernels $K_{vcv'c'}$ for which $v$ or $v'$ are in the 4*d* subspace (i.e., when $v$ or $v'$ ranges from 1 to 10 in $Ag_2$). This means that the only optical excitations that are computed in this thought experiment are those associated with HOMO of largely *s* character, which can then be compared, for example, with the HOMO →LUMO and HOMO→LUMO+1 transitions discussed above. The results for $Ag_2$ are shown in Fig. 4, where we readily see the quenching and redshift effects due to *d* electrons, as the two main low-energy lines are blueshifted and their brightness enhanced when the 4*d* orbitals are removed from the system. A similar effect is observed for the Ag atom as well. These observations can be explained by screening due to *d* electrons, i.e., the *d* electrons are polarizable and they screen the electromagnetic field acting on *s* electrons. Without *d* electrons, the electromagnetic field is stronger, and hence the absorption lines are brighter. It is interesting to observe that once the *d* electrons are removed from the system, the excitation energies computed within TDLDA and *GW*BSE are almost the same, although differences remain in the computed oscillator strengths.

Another aspect unveiled by our thought experiment is that, after 4*d* electrons are removed, the *GW*BSE lines blueshift and glow more than TDLDA lines do. This could be a manifestation of nonlocality of the *GW*BSE kernel. As discussed in Sec. II D, the BSE equation is similar to Casida's equations for TDLDA, but there are two new aspects in the BSE: the lack of self-interaction and nonlocality. Self-interaction is absent in *GW*BSE. It is a spurious effect of the LDA and it is largely responsible for an underestimation of the electronic gap (separation between occupied and unoccupied orbitals).[21] Nonlocality means that interactions among electron-hole pairs are described by a screened Coulomb kernel [Eq. (16)], which is strongly nonlocal compared to the LDA kernel [Eq. (6)]. Typically, the screened kernel contains a very strong electrodynamic attraction between the electron and the hole. Screening in small clusters is expected to be weak because there are few valence electrons in the system. In addition, the screened Coulomb kernel is essentially nonlocal. One electron at point $\mathbf{r}$ is attracted by a hole at point $\mathbf{r}'$ through the screened potential $W(\mathbf{r},\mathbf{r}')$. At very short distances, this potential is very similar to the electrostatic Coulomb potential $e^2/|\mathbf{r}-\mathbf{r}'|$. At longer distances, it is weakened by the polarization field induced in the medium. In contrast, the LDA kernel is strictly local. In $Ag_n$ clusters, nonlocality enhances correlations between 4*d* electrons and the other electrons. When those correlations are eliminated by removing 4*d* electrons, the low-energy lines in the *GW*BSE spectrum are enhanced significantly.

We can now interpret the increased deterioration of the present *GW*BSE results as compared to experimental data in $Ag_n$ clusters in going from $n$=1–2 to $n$=3–8 as a combination of three factors: (1) low energy optical transitions in silver clusters have been reported to have significant *d* character.[12,47] In contrast, the first two optical lines of Ag and $Ag_2$ involve molecular orbitals derived primarily from the 5*s* atomic orbital. (2) Our thought experiment indicates that *GW*BSE absorption lines are more sensitive to correlations involving 4*d* electrons. (3) By calculating self-energies using a pseudopotential that places semicore orbitals in the core, exchange-correlation effects between 4*d* and semicore orbitals are ignored. This results in inaccurate predictions for the *GW* quasiparticle energies, which in turn significantly affect the BSE predictions for the optical spectra.

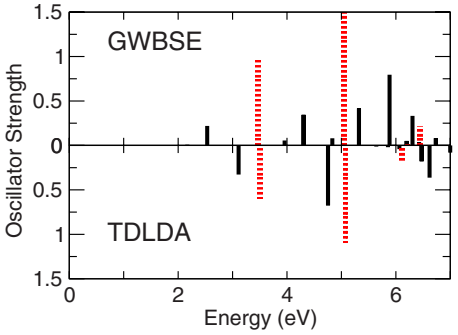


FIG. 4. (Color online) Oscillator strengths of low-energy excitations in $Ag_2$ computed by removing transitions involving 4*d* orbitals (red dashed lines) and by following the standard methodology (solid lines) within *GW*BSE (upper panel) and TDLDA (lower panel).

## V. DISCUSSION

Owing to the complexity of the quantum many-body problem, practical implementations of the *GW*BSE method usually involve a number of approximations in order to make its applications to real systems computationally manageable. In this section, we discuss some of these approximations in terms of their validity in the particular case of clusters of silver atoms.

### A. Satellites and the quasiparticle approximation

Electrons in a real material interact among themselves and form an entangled state where the concept of single-electron dynamics becomes nontrivial. Within the Fermi liquid theory,[25] electrons are replaced with quasiparticles (quasielectrons and holes), which are entities with long lifetimes and well defined energies. The Fermi-liquid theory, upon which the *GW*A is built, relies on the fact that the imaginary part of the self-energy for those particles is small. In that case, their lifetime (essentially the inverse of that imaginary part) will be long compared to other relevant time scales. One valid question is whether the quasiparticle approximation is still valid in small $Ag_n$ clusters. We address this question by calculating directly the imaginary part of the self-energy for some of the clusters studied.

The upper panel of Fig. 5 depicts the self-energy evaluated at the HOMO and the LUMO of Ag and $Ag_2$,

$$\Sigma_n(E) = \int d\mathbf{r}d\mathbf{r}'\,\varphi_n(\mathbf{r})\Sigma(\mathbf{r},\mathbf{r}';E)\varphi_n(\mathbf{r}'). \tag{19}$$

In all cases, the real part is smooth in the vicinity of the quasiparticle energy. In both systems, there is a satellite structure either a couple of eVs below the HOMO or above the LUMO. The imaginary part has similar behavior. It is smooth around the quasiparticle energy and grows at energies below the HOMO and above the LUMO. The slope of the self-energy is related to the renormalization factor,[4,27]

$$z_n = \left[1 - \left.\frac{\partial\Sigma}{\partial E}\right|_{E_n}\right]^{-1}. \tag{20}$$

The computed renormalization factors for the atom and the dimer are 0.83 (HOMO, Ag), 0.80 (LUMO, Ag), 0.81 (HOMO, $Ag_2$), and 0.84 (LUMO, $Ag_2$). For the rest of the clusters, the factor ranges from 0.7 to 0.9.

A quantity related to the Green's function is the spectral function,[5,27]

$$A(\mathbf{r},\mathbf{r}';E) = \frac{1}{\pi}|\mathrm{Im}\,G(\mathbf{r},\mathbf{r}';E)|. \tag{21}$$

In the quasiparticle approximation, the spectral function for a given electronic orbital has a very sharp peak at the quasiparticle energy. Its width is equal to the imaginary part of the self-energy at $E=E_n$. For the clusters studied, the imaginary part is usually less than 0.1 eV for reasonable values of the broadening parameter. The integral under the peak is equal to $z_n$. Our calculations indicate that the calculated Green's function is consistent with the quasiparticle approximation in that there is a quasiparticle peak. Its weight is around 70% to 90% of the total spectral weight. The remaining spectral weight stays at the satellites. Figure 5 shows that the spectral function has very low but finite amplitude in the satellite region. The energy separation between the satellite region and the quasiparticle peak is dictated by the position of poles in the polarizability.

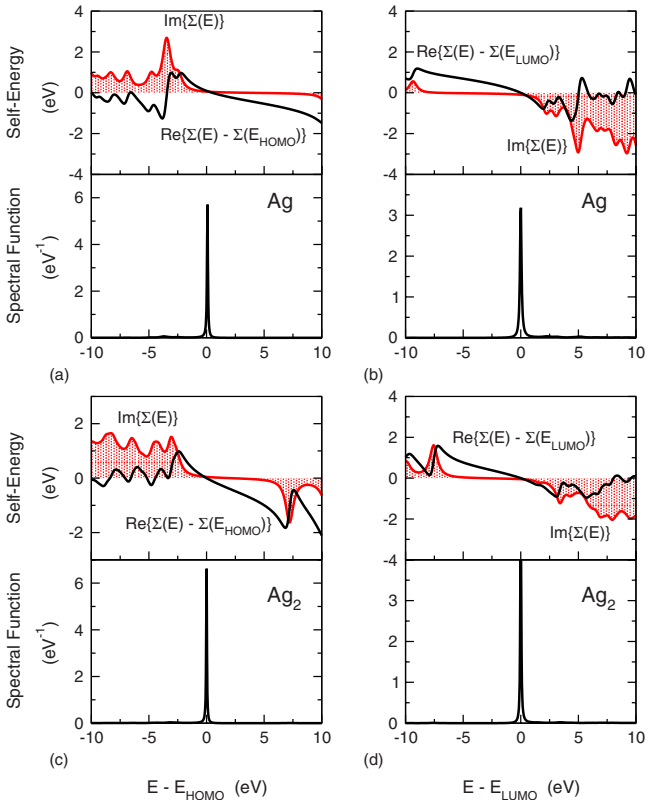


FIG. 5. (Color online) Self-energy (upper panel) and spectral function (lower panel) evaluated at (a) Ag HOMO, (b) Ag LUMO, (c), $Ag_2$ HOMO, and (d) $Ag_2$ LUMO. The upper panel of each subfigure shows the real part in a (black) continuous line and the imaginary part in a (red) continuous, shaded line. For better visualization, the real part is shifted by a constant so that it is zero when the horizontal axis is zero. Kohn-Sham wave functions were used in this figure. In the calculations, we removed the singularities in the energy denominators of Eq. (1) by adding 0.4 eV to the imaginary part. As a result, the calculated spectral function and self-energy have broadened singularities.

### B. Self-consistency

The importance of self-consistency in the *GW*A has been investigated in bulk materials,[4,48] where band gaps have been observed to increase when self-energy, Green's function, and polarizability are calculated self-consistently by iterating Eqs. (7)–(9). The amount of gap opening is highly sensitive to how self-consistency is imposed. The same gap opening has been observed in isolated molecules as well.[49] In addition, non-self-consistent calculations have been shown to give inaccurate results in strongly correlated transition-metal oxides, such as NiO and MnO.[48,50–52]

Given that our non-self-consistent *GW*BSE results for the isolated silver atom and for $Ag_2$ are consistent with experi-

TABLE IV. Quasiparticle energies of HOMO and LUMO, and the resulting HOMO-LUMO gaps in Ag and $Ag_2$ calculated within various vertex approximations. In all cases, quasiparticle orbitals were assumed equal to DFT orbitals and $G$ was taken as the DFT Green's function. The values reported under the column marked with "$G_0W_f$ no vertex" were obtained by dropping the last integral in Eq. (12). All energies are in eV.

| | | $G_0W_0$ | $G_0W_f$ (No vertex) | $G_0W_f$ |
|---|---|---|---|---|
| Ag | HOMO | −8.01 | −8.07 | −7.53 |
| | LUMO | −1.79 | −2.12 | −1.26 |
| | Gap | 6.22 | 5.95 | 6.27 |
| $Ag_2$ | HOMO | −7.94 | −7.80 | −7.54 |
| | LUMO | −1.57 | −1.42 | −1.12 |
| | Gap | 6.37 | 6.38 | 6.42 |

mental data to within a fraction of eV, one might expect self-consistency to be of little importance. We have calculated quasiparticle energies of Ag and $Ag_2$ using partial self-consistency, in which the quasiparticle wave functions were kept equal to DFT wave functions and only their energies were allowed to change during iterations of $\Sigma$, $G$, and $\Pi$. With this procedure, the IP of each system changed by less than 0.2 eV. On the other hand, the EA decreased significantly, from 1.26 to 0.5 eV for Ag, and from 1.12 to 0.6 eV for $Ag_2$. The reason for this behavior is a competition between screening and renormalization. Self-consistency reduces static screening and, if dynamical effects are ignored, leads to higher self-energy [recall that the polarizability in Eq. (12) is negative, therefore weak screening means larger $\Pi_f$]. At the same time, the renormalization factor also increases, leading to a reduction in the slope $\partial\Sigma/\partial E$, and hence, lower self-energies at occupied orbitals and higher self-energies at unoccupied orbitals. The two effects partially cancel each other at the HOMO, and they add up at the LUMO. In both cases, self-consistency resulted in electron affinities much smaller than the experimental values, with a discrepancy of at least 0.5 eV. More refined self-consistent schemes, possibly with the inclusion of the satellite structure, could lead to smaller errors.[39] The issue of self-consistency in the context of the *GW*BSE method for real materials is not yet fully understood and it is being actively investigated.[4,48]

### C. Vertex corrections

Equation (11) assumes a local and adiabatic approximation to the vertex operator, which explicitly enters into the equations for both the polarizability and the self-energy.[4,27] For consistency, the same vertex should be used to compute both quantities. That is, Eq. (9) should be used with the RPA polarizability and Eq. (12) should be used with the TDLDA polarizability. However, since neither equation is exact, one could try different combinations. In Table IV, we compare the approximations $G_0W_0$ and $G_0W_f$ with a third approximation, where we use the TDLDA polarizability but remove the last integral in Eq. (12), which contains purely vertex terms. Replacing the RPA polarizability with the TDLDA polarizability does not seem to affect quasiparticle energies much, except for the HOMO of Ag which shifts down from −1.79 to −2.12 eV. The HOMO-LUMO gap itself decreases in Ag and remains virtually unchanged in $Ag_2$. Inclusion of explicit vertex terms increases the quasiparticle energies of all orbitals in Table IV. Surprisingly, explicit vertex terms increase the HOMO-LUMO gap of Ag, almost canceling the effect of polarizability. Between $G_0W_0$ and $G_0W_f$ approximations, the HOMO-LUMO gap remains unchanged within the numerical accuracy. Given the robustness of the HOMO-LUMO gap between the $G_0W_0$ and $G_0W_f$ approximations, we report in Fig. 2 only the spectra obtained using the $G_0W_f$. Spectra obtained with $G_0W_f$-BSE and $G_0W_0$-BSE have been shown to be almost identical in the visible and low ultraviolet range.[13] We note that in this work we assumed an "LDA-like" form for the vertex terms. This approximation seems to produce accurate predictions of the ionization potential of molecules.[13,49] More accurate vertex terms could be designed, but their form is presently unknown.

## VI. SUMMARY

In summary, we have computed and analyzed the electronic and optical excitations in $Ag_n$ clusters, $n=1-8$, within density-functional ($\Delta$SCF and TDLDA) as well as many-body (GW+BSE) theories. The ionization potentials and electron affinities of $Ag_n$ as predicted within the *GW*A are generally in good agreement with experimental values (within a fraction of an eV), as the corresponding quasiparticle orbitals (HOMO and LUMO) are predominantly of $s(p)$ character. For molecular orbitals of increased $d$ character, good agreement with experimental values is possible only if $4s$ and $4p$ semicore atomic orbitals, which have a significant spatial overlap with $4d$ atomic orbitals, are included as part of the valence in the *GW* computations. Otherwise, the large exchange-correlation interactions among $4s$, $4p$, and $4d$ orbitals result in significant errors in the *GW* quasiparticle energies and the associated optical excitations. The importance of these interactions in the band structure of semiconductors was uncovered in previous studies, both in the context of the pseudopotential approximation[39,40] and in all-electron calculations.[53] Our computations and analyses of the optical excitation energies and the associated oscillator strengths of $Ag_n$ show that correlations involving $d$ electrons give rise to quenching of the oscillator strengths of low-energy excitations. This quenching is significantly more pronounced in the computations based on solving the BSE than in time-dependent DFT. In general, TDLDA gives rise to excitation energies which are in reasonably good agreement with experimental values. While *GW*BSE seems to give good results for low-energy ($s\rightarrow p$) excitations in the Ag atom, even a small amount of $d$ character in the associated quasiparticle wave functions, as is the case even at low energies as size increases, results in poor agreement of the *GW*BSE results with experiment, owing to the inclusion of strong nonlocality effects in the BSE methodology.

## ACKNOWLEDGMENTS

This work was supported by the U.S. Department of

Energy Grant Nos. DE-FG02-06ER46286, DE-FG02-06ER15760 (M.L.T. and J.R.C.), and DE-FG02-03ER15488 (J.C.I. and S.Ö.), by the National Science Foundation Grant No. DMR-0551195 (M.L.T. and J.R.C.), by the Office of Basic Energy Sciences, Division of Chemical Sciences, Geosciences, and Biosciences, under Contract No. DE-AC-02-06CH11357 (J.J.), and facilitated by the DOE Computational Materials Science Network. Research at the Oak Ridge National Laboratory was sponsored by the Division of Materials Sciences and Engineering, Office of Basic Energy Sciences, U.S. Department of Energy, under Contract No. DE-AC05-00OR22725 with UT-Battelle, LLC. This research used resources of NERSC, which is supported by the Office of Science of the U.S. Department of Energy.

[1] M. Petersilka, U. J. Gossmann, and E. K. U. Gross, Phys. Rev. Lett. **76**, 1212 (1996).
[2] M. E. Casida, in *Recent Advances in Density-Functional Methods, Part I*, edited by D. P. Chong (World Scientific, Singapore, 1995), p. 155.
[3] M. E. Casida, in *Recent Developments and Applications of Modern Density Functional Theory*, edited by J. M. Seminario (Elsevier, Amsterdam, 1996), p. 391.
[4] W. Aulbur, L. Jönsson, and J. Wilkins, in *Solid State Physics*, edited by F. Seitz, D. Turnbull, and H. Ehrenreich (Academic, New York, 2000), Vol. 54, p. 1.
[5] M. S. Hybertsen and S. G. Louie, Phys. Rev. B **34**, 5390 (1986).
[6] M. Rohlfing and S. G. Louie, Phys. Rev. B **62**, 4927 (2000).
[7] G. Onida, L. Reining, and A. Rubio, Rev. Mod. Phys. **74**, 601 (2002).
[8] L. Reining, V. Olevano, A. Rubio, and G. Onida, Phys. Rev. Lett. **88**, 066404 (2002).
[9] I. Vasiliev, S. Öğüt, and J. R. Chelikowsky, Phys. Rev. Lett. **82**, 1919 (1999).
[10] K. Yabana and G. F. Bertsch, Phys. Rev. A **60**, 3809 (1999).
[11] I. Vasiliev, S. Öğüt, and J. R. Chelikowsky, Phys. Rev. B **65**, 115416 (2002).
[12] J. C. Idrobo, S. Öğüt, and J. Jellinek, Phys. Rev. B **72**, 085445 (2005).
[13] M. L. Tiago and J. R. Chelikowsky, Phys. Rev. B **73**, 205334 (2006).
[14] K. Baishya, J. C. Idrobo, S. Öğüt, M. L. Yang, K. Jackson, and J. Jellinek, Phys. Rev. B **78**, 075439 (2008).
[15] M. Harb, F. Rabilloud, D. Simon, A. Rydlo, S. Lecoultre, F. Conus, V. Rodrigues, and C. Félix, J. Chem. Phys. **129**, 194108 (2008).
[16] E. K. U. Gross, J. F. Dobson, and M. Petersilka, in *Density Functional Theory*, edited by R. F. Nalewajski (Springer-Verlag, Berlin, 1996), p. 81.
[17] K. Burke, M. Petersilka, and E. K. U. Gross, in *Recent Advances in Density Functional Methods*, edited by P. Fantucci and A. Bencini (World Scientific, Singapore, 2002), Vol. III, p. 67.
[18] J. R. Chelikowsky, N. Troullier, and Y. Saad, Phys. Rev. Lett. **72**, 1240 (1994).
[19] J. R. Chelikowsky, N. Troullier, K. Wu, and Y. Saad, Phys. Rev. B **50**, 11355 (1994).
[20] D. M. Ceperley and B. J. Alder, Phys. Rev. Lett. **45**, 566 (1980).
[21] J. P. Perdew and A. Zunger, Phys. Rev. B **23**, 5048 (1981).
[22] Y. Zhou, Y. Saad, M. L. Tiago, and J. R. Chelikowsky, Phys. Rev. E **74**, 066704 (2006).
[23] S. Srinivas, U. A. Salian, and J. Jellinek, in *Metal-Ligand Interactions in Biology, Chemistry and Physics*, edited by N. Russo and D. R. Salahub (Kluwer, Dordrecht, 2000), p. 295.
[24] M. S. Hybertsen and S. G. Louie, Phys. Rev. B **35**, 5585 (1987).
[25] A. L. Fetter and J. D. Walecka, *Quantum Theory of Many-Particle Systems* (Mc-Graw Hill, New York, 1971).
[26] E. L. de la Grandmaison, S. B. Gowda, Y. Saad, M. L. Tiago, and J. R. Chelikowsky, Comput. Phys. Commun. **167**, 7 (2005).
[27] L. Hedin and S. Lundqvist, in *Solid State Physics*, edited by F. Seitz, D. Turnbull, and H. Ehrenreich (Academic, New York, 1969), Vol. 23, p. 1.
[28] R. DelSole, L. Reining, and R. W. Godby, Phys. Rev. B **49**, 8024 (1994).
[29] A. J. Morris, M. Stankovski, K. T. Delaney, P. Rinke, P. García-González, and R. W. Godby, Phys. Rev. B **76**, 155106 (2007).
[30] L. Reining, G. Onida, and R. W. Godby, Phys. Rev. B **56**, R4301 (1997).
[31] C. Jackschath, I. Rabin, and W. Schulze, Z. Phys. D. **22**, 517 (1992).
[32] G. Alameddin, J. Hunter, D. Cameron, and M. M. Kappes, Chem. Phys. Lett. **192**, 122 (1992).
[33] J. Ho, K. M. Ervin, and W. C. Lineberger, J. Chem. Phys. **93**, 6987 (1990).
[34] K. J. Taylor, C. L. Pettiette-Hall, O. Chesnovsky, and R. E. Smalley, J. Chem. Phys. **96**, 3319 (1992).
[35] H. Handschuh, C. Y. Cha, P. S. Bechthold, G. Ganteför, and W. Eberhardt, J. Chem. Phys. **102**, 6406 (1995).
[36] S. Öğüt, J. R. Chelikowsky, and S. G. Louie, Phys. Rev. Lett. **79**, 1770 (1997).
[37] N. Troullier and J. L. Martins, Phys. Rev. B **43**, 1993 (1991).
[38] M. Rohlfing, P. Krüger, and J. Pollmann, Phys. Rev. Lett. **75**, 3489 (1995).
[39] M. Rohlfing, P. Krüger, and J. Pollmann, Phys. Rev. B **56**, R7065 (1997).
[40] E. L. Shirley, X. Zhu, and S. G. Louie, Phys. Rev. B **56**, 6648 (1997).
[41] E. L. Shirley and R. M. Martin, Phys. Rev. B **47**, 15404 (1993).
[42] E. L. Shirley and R. M. Martin, Phys. Rev. B **47**, 15413 (1993).
[43] C. L. Reis, J. M. Pacheco, and J. L. Martins, Phys. Rev. B **68**, 155111 (2003).
[44] S. Fedrigo, W. Harbich, and J. Buttet, Phys. Rev. B **47**, 10706 (1993).
[45] F. Conus, J. T. Lau, V. Rodrigues, and C. Félix, Rev. Sci. Instrum. **77**, 113103 (2006).
[46] M. D. Morse, Chem. Rev. **86**, 1049 (1986).
[47] J. C. Idrobo, S. Öğüt, and J. Jellinek, Phys. Rev. B **77**, 239901(E) (2008).
[48] T. Kotani, M. van Schilfgaarde, and S. V. Faleev, Phys. Rev. B **76**, 165106 (2007).
[49] M. L. Tiago, P. R. C. Kent, R. Q. Hood, and F. A. Reboredo, J. Chem. Phys. **129**, 084311 (2008).

[50] S. Massidda, A. Continenza, M. Posternak, and A. Baldereschi, Phys. Rev. B **55**, 13494 (1997).
[51] F. Aryasetiawan and O. Gunnarsson, Phys. Rev. Lett. **74**, 3221 (1995).
[52] J.-L. Li, G.-M. Rignanese, and S. G. Louie, Phys. Rev. B **71**, 193102 (2005).
[53] M. van Schilfgaarde, T. Kotani, and S. Faleev, Phys. Rev. Lett. **96**, 226402 (2006).